Publication Year	2017
Acceptance in OA	2020-10-26T08:39:46Z
Title	The cool-core state of Planck SZ-selected clusters versus X-ray-selected samples: evidence for cool-core bias
Authors	ROSSETTI, MARIACHIARA, GASTALDELLO, FABIO, Eckert, D., Della Torre, M., Pantiri, G., Cazzoletti, P., MOLENDI, SILVANO
Publisher's version (DOI)	10.1093/mnras/stx493
Handle	http://hdl.handle.net/20.500.12386/27981
Journal	MONTHLY NOTICES OF THE ROYAL ASTRONOMICAL SOCIETY
Volume	468

Monthly Notices
of the
ROYAL ASTRONOMICAL SOCIETY

MNRAS **468,** 1917–1930 (2017) doi:10.1093/mnras/stx493
Advance Access publication 2017 February 24

The cool-core state of Planck SZ-selected clusters versus X-ray-selected samples: evidence for cool-core bias

M. Rossetti,[1,2]⋆ F. Gastaldello,[1] D. Eckert,[3] M. Della Torre,[2] G. Pantiri,[2] P. Cazzoletti[2,4] and S. Molendi[1]

[1] *INAF, Istituto di Astrofisica Spaziale e Fisica Cosmica, via Bassini 15, I-20133 Milano, Italy*
[2] *Dipartimento di Fisica, Università degli Studi di Milano, via Celoria 16, I-20133 Milano, Italy*
[3] *Department of Astronomy, University of Geneva, 16, Ch. d'Ecogia, CH-1290 Versoix, Switzerland*
[4] *Max Planck Institute for Extraterrestrial Physics, Giessenbachstraße, D-85748 Garching, Germany*

Accepted 2017 February 22. Received 2017 February 22; in original form 2016 December 22

ABSTRACT

We characterized the population of galaxy clusters detected with the Sunyaev–Zeldovich (SZ) effect with *Planck* by measuring the cool-core state of the objects in a well-defined subsample of the Planck SZ catalogue. We used as an indicator the concentration parameter. The fraction of cool-core clusters is 29 ± 4 per cent and does not show significant indications of evolution in the redshift range covered by our sample. We compare the distribution of the concentration parameter in the Planck sample with the one of the X-ray selected sample MACS: the distributions are significantly different and the cool-core fraction in MACS is much higher (59 ± 5 per cent) than that in Planck. Since X-ray-selected samples are known to be biased towards cool cores due to the presence of their prominent surface brightness peak, we simulated the impact of the 'cool-core bias'. We found that this bias plays a large role in the difference between the fractions of cool cores in the two samples. We examined other selection effects that could in principle bias SZ surveys against cool cores, but we found that their impact is not sufficient to explain the difference between Planck and MACS. The population of X-ray underluminous objects, which are found in SZ surveys but missing in X-ray samples, could possibly contribute to the difference, as we found most of them to be non-cool cores, but this hypothesis deserves further investigation.

Key words: galaxies: clusters: general – galaxies: clusters: intracluster medium.

1 INTRODUCTION

It is often difficult to derive the statistical properties of a population of celestial sources from an observed sample that is a particular realization of the underlying population. Indeed, one has to be sure that the sample under analysis is representative and unbiased with respect to selection effects; that is, the method that was used to detect objects, and eventually to further select them, does not influence the properties that we want to analyse. Galaxy clusters are no exception to this rule.

Ever since the beginning of X-ray astronomy, X-ray observations have provided an efficient way to detect and characterize clusters. Many cluster catalogues (i.e. REFLEX, Böhringer et al. 2004; NORAS, Böhringer et al. 2000; HIFLUGCS, Reiprich & Böhringer 2002; REXCESS, Böhringer et al. 2007; MACS, Ebeling, Edge & Henry 2001) have been built based on the *ROSAT* All Sky Survey (RASS), which was excellent in terms of sky coverage but limited in depth. X-ray surveys aimed at detecting extended sources, such as galaxy clusters, may become 'surface brightness limited' rather than 'flux limited' at faint fluxes (Rosati, Borgani & Norman 2002; Pierre et al. 2016). Indeed, realistic X-ray surveys can detect extended objects up to a 'detection radius' where they exceed the background level. It is thus easier to detect a cluster with a prominent surface brightness peak than an object with a shallower profile, even if they have the same flux when integrated to a physically relevant radius (i.e. R_{500}), typically larger than the detection radius. This selection bias that affects X-ray surveys of galaxy clusters is also known as 'cool-core bias' (Eckert et al. 2011), and it was early recognized in the first *Einstein* surveys of galaxy clusters (Pesce et al. 1990 and references therein). 'Cool core' (CC hereafter) clusters are observationally characterized by a prominent central surface brightness peak associated with a temperature decrease in the inner regions and are usually considered as relaxed objects. Eckert et al. (2011) have shown that their number is overestimated in X-ray-selected cluster samples (HIFLUGCS) because of their prominent surface brightness peak. A further bias is due to the higher luminosity of CC clusters with respect to

---

⋆ E-mail: rossetti@iasf-milano.inaf.it

Published by Oxford University Press on behalf of the Royal Astronomical Society

non-cool cores (NCC) at a given mass, which makes the detection rate of CC higher than fainter NCC objects, in a flux-limited sample suffering from the Malmquist bias (Hudson et al. 2010). Thus, the ratio between CC and NCC objects, which depends strongly on CC formation scenarios and on the models of cluster evolution, is likely overestimated in X-ray-selected samples.

Over the last decade, an alternative method to search for galaxy clusters has received growing attention: the Sunyaev–Zeldovich effect (SZ hereafter; Sunyaev & Zeldovich 1970, 1972), with the publications of the first large catalogues of galaxy clusters from different experiments, containing from 100 to more than 1000 objects (Hasselfield et al. 2013; Bleem et al. 2015; Planck Collaboration XXIX 2014; Planck Collaboration XXVII 2016). The SZ surface brightness does not depend on the redshift of the source, allowing us in principle to detect all the clusters in the Universe above a given signal, regardless of their distance, and to build virtually mass-limited samples of galaxy clusters. Actually the finite spatial resolution of real instruments limits the detection of the most distant objects (especially for Planck whose lowest energy channel used for SZ measurement has a beam size of 10 arcmin) but the distribution of clusters in the mass–redshift plane is definitely flatter for SZ-selected samples than for X-ray samples. Indeed, SZ surveys have detected more than 450 clusters at $z > 0.5$, significantly increasing the number of known objects in this redshift range, which was limited to a few tens of clusters in X-ray catalogues before them (75 in MCXC; Piffaretti et al. 2011).

Simulations have shown that SZ quantities do not strongly depend on the dynamical state of the clusters (Motl et al. 2005), showing only a modest effect of less than 10 per cent due to mergers (Battaglia et al. 2012; Krause et al. 2012). This is supported observationally by the small scatter in the scaling relation between the SZ total signal Y and the mass (e.g. see Planck Collaboration XX 2014 and references therein). Moreover, Planck Collaboration XXVII (2016) showed with Monte Carlo simulations that the morphology of the source, which is in general more irregular and disturbed for interacting systems, has negligible impact in the detection procedure in the *Planck* survey. In principle, CC bias may play a role also in SZ surveys: CC clusters feature a prominent peak in the pressure profiles (Planck Collaboration V 2013), which results in an increase in the central value of the Comptonization parameter $y \propto \int P dl$ (Pipino & Pierpaoli 2010). However, simulations have shown this effect to be small, especially for Planck whose beam size is larger than the typical cluster size and is more sensitive to the total SZ signal rather than to its central value (Pipino & Pierpaoli 2010; Lin et al. 2015).

In a recent paper (Rossetti et al. 2016, Paper I hereafter), we showed that the dynamical state of Planck SZ-selected clusters is significantly different than in X-ray surveys. We measured an indicator of dynamical activity ($D_{\mathrm{X,BCG}}$, the projected offset between the position of the X-ray peak and the one of the brightest cluster galaxy) for a representative subsample of Planck clusters (Planck Collaboration XX 2014), and we compared its distribution to the one of the same indicator in several X-ray-selected samples available in the literature. The distributions are significantly different and the fraction of dynamically relaxed objects is smaller in the Planck sample than in X-ray-selected samples, confirming the early impression that many *Planck*-selected objects are dynamically disturbed systems (Planck Collaboration IX 2011). In Paper I, we suggested that the origin of this discrepancy may be due to the CC bias affecting X-ray surveys, since dynamically relaxed objects usually host CCs. However, we could not verify this hypothesis as $D_{\mathrm{X,\,BCG}}$ is not a direct indicator of the presence of a peaked surface brightness profile, although it shows correlations with several CC indicators (Sanderson, Edge & Smith 2009). To test this hypothesis, one would need to measure the presence and strength of the surface brightness peak in large SZ and X-ray samples and compare them. A first result in this direction has been presented by Semler et al. (2012), who measured the concentration parameter (Santos et al. 2008), a CC indicator directly related to the strength of the surface brightness peak, a small sample of 13 clusters detected with the South Pole Telescope (SPT). They compare the distribution of this indicator in their sample with the one in the X-ray-selected 400d sample (Burenin et al. 2007) and found them to be consistent, but given their small number of objects, they could constrain only the fraction of CCs between 7 and 59 per cent. More recently, McDonald et al. (2013) measured the concentration parameter, as well as other CC indicators, for a larger SPT sample but do not directly make a comparison with X-ray samples. Although it was not the main objective of their paper, Mantz et al. (2015) provided a first significant result, finding that the fraction of objects with a peaked surface brightness profile is significantly higher in X-ray-selected samples than in SZ samples, using SPT and a small (30 objects) subset of the early Planck catalogue (Planck Collaboration VIII 2011). Conversely, the recent comparison by Nurgaliev et al. (2016) between the SPT SZ sample and the X-ray-selected 400d catalogue (Burenin et al. 2007) does not address directly the role of CC bias as it is based on morphological indicators that measure the deviation from symmetry of the cluster images and thus compare the dynamical state, as we have also done in Paper I.

The aim of this paper is to directly address the origin of the discrepancy in the dynamical state that we found in Paper I and to test the hypothesis that it is due to the CC bias. We use as a CC indicator the concentration parameter (Santos et al. 2008), since it directly measures the strength of the surface brightness peak. We measure it for a large sample of SZ-selected clusters drawn from the Planck catalogue and consistently for the X-ray-selected MACS sample (Mann & Ebeling 2012). The outline of the paper is as follows. In Section 2, we present our samples, while in Section 3, we describe the reduction and analysis of *Chandra* and *XMM–Newton* data that we applied to both samples. We present our results and compare the distributions in Section 4, comparing it also with previous results and other samples available in the literature. In Section 5, we discuss the role of CC bias, trying to reproduce our results with simulations. Finally, we discuss other possibilities in Section 6. In this paper, we assume a Λ-CDM cosmology with $H_0 = 70$ km s^{-1} Mpc^{-1}, $\Omega_{\mathrm{m}} = 0.3$ and $\Omega_\Lambda = 0.7$.

2 THE SAMPLES

2.1 Planck cluster sample

The starting point of our SZ-selected sample is the Planck cosmology sample (PSZ1-cosmo), which has been used for the cosmological analysis with cluster number counts described in Planck Collaboration XX (2014). It is a high-purity subsample built from the first release of the Planck catalogue of SZ sources (Planck Collaboration XXIX 2014), containing all the detection with the highest signal-to-noise ratio (S/N > 7) after the application of a mask, that excludes the galactic plane and point sources and leaves 65 per cent of the sky for the survey. It contains 189 clusters: all of them have been confirmed at other wavelengths, and redshifts have been associated with each cluster. The properties of the sample and its completeness are described in detail in Planck Collaboration XX (2014). The PSZ1-cosmo sample has been almost completely

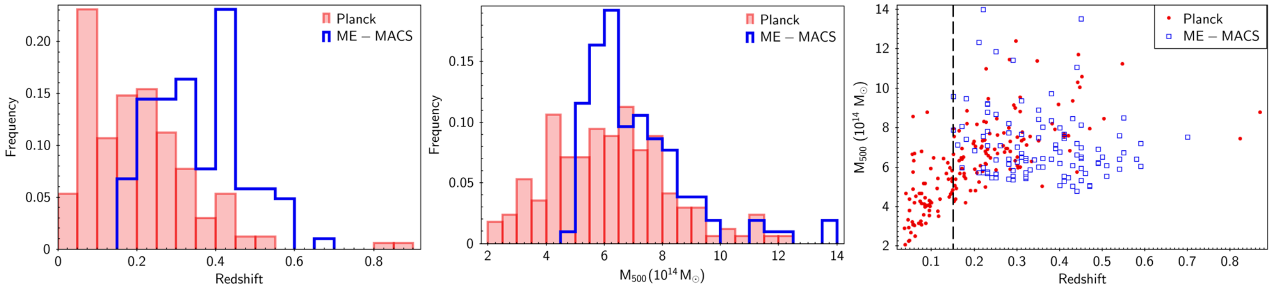

Figure 1. Distribution of redshift (left), mass (middle) and *M*–*z* plane (right) in the Planck and ME-MACS samples.

followed up in X-rays with either *Chandra* or *XMM–Newton* and is thus the ideal starting point to measure the concentration parameter (Section 3.3) of *Planck*-selected objects. The larger and more recent second release of the Planck SZ catalogue (PSZ2; Planck Collaboration XXVII 2016) has not benefited yet of a similar follow-up campaign and the analysis of this sample would thus be strongly incomplete.

We used *Chandra* data as a reference because they are better suited for the measurement of concentration parameters, given the excellent spatial resolution. We measured concentration parameters for 154 objects with *Chandra* at $z > 0.07$, using this redshift as a lower limit to accommodate 400 kpc within the *Chandra* ACIS-I field of view. For 10 objects at $z > 0.07$, we measured concentration parameters with the *XMM–Newton* data, as *Chandra* data were not available in the archive. For five objects in the redshift range 0.03–0.07, we used *XMM–Newton* data, exploiting its larger field of view to cover the cluster region used in the definition of the concentration parameter (Section 3.3). The remaining objects for which observations are potentially available but not used here are: eight clusters with *Chandra* data planned or still proprietary as of 2016 July, four clusters with *XMM–Newton* data at $z < 0.03$ (not completely covered even with *XMM–Newton*) and four clusters at $z > 0.35$, for which the core region used in our indicator is not resolved with *XMM–Newton* (Section 3.3).

Our final sample is thus composed of 169 clusters in the redshift range 0.04–0.87 with a median $z = 0.18$ and in the mass range $(2–12) \times 10^{14}\,\mathrm{M_{\odot}}$ (median $M_{500} = 6.2 \times 10^{14}\,\mathrm{M_{\odot}}$).

2.2 MACS sample

In Paper I, we compared the distribution of our dynamical indicator in the Planck sample with the one of three X-ray-selected samples (HIFLUGCS, REXCESS and MACS). We showed that MACS is the most suited for the comparison with Planck among those samples, since its redshift and mass distributions are more similar to the ones of the PSZ1-cosmo sample. Actually, the sample that we used in Paper I is not the original MACS sample (whose selection criteria are described in Ebeling et al. 2001) but its extended version is described in Mann & Ebeling 2012 (ME-MACS hereafter). Both MACS and ME-MACS are drawn from the RASS Bright Source Catalogue (Voges et al. 1999), with a flux limit $f_{\mathrm{RASS}}[0.1–2.4\,\mathrm{keV}] > 1 \times 10^{-12}\,\mathrm{erg\,cm^{-2}\,s^{-1}}$. The main difference is that MACS is limited by definition to the most distant systems ($z > 0.3$), while ME-MACS extends to lower redshifts ($z > 0.15$) and has an additional luminosity cut $L_{\mathrm{RASS}}[0.1–2.4\,\mathrm{keV}] > 5 \times 10^{44}\,\mathrm{erg\,s^{-1}}$. The ME-MACS sample is a well-defined purely X-ray-selected sample, based on a flux-limited survey, and it is thus well suited for a comparison between the X-ray and SZ selection. Moreover, its redshift distribution is more similar to the redshift distribution of the Planck sample with respect to the original MACS and we thus decided to use it in our analysis. Finally, 104 out of the 129 clusters meeting the ME-MACS selection (listed in Mann & Ebeling 2012) have public *Chandra* observations that we used to measure the concentration parameter (Section 3.3).

2.3 Mass and redshift distributions

In Fig. 1, we show the redshift and mass distributions of the Planck and ME-MACS samples. As in Paper I, we estimate the masses of the ME-MACS clusters, using the *L*–*M* scaling relation in Pratt et al. (2009). By construction, the minimum redshift of the ME-MACS sample is 0.15, thus the median value of the ME-MACS sample ($z = 0.35$) is larger than that in the PSZ1 sample and the two distributions are significantly different. Also the mass distributions appear different: objects with $M < 5 \times 10^{14}\,\mathrm{M_{\odot}}$ are found only in the Planck sample and correspond to the low-redshift objects that are missing by construction in ME-MACS. To minimize the difference in the two samples, we define a subsample of the Planck catalogue by imposing $z > 0.15$: with this choice we have a subsample of 103 objects, with median redshift 0.25 and median mass $7.1 \times 10^{14}\,\mathrm{M_{\odot}}$.

3 DATA ANALYSIS

3.1 *Chandra* data reduction

We analysed *Chandra* data with the CIAO software 4.6, using CALDB version 4.6.1, reprocessing data from the level 1 event files and following the standard data reduction threads.[1] We reprocessed event files, using the `chandra_repro` tool with standard corrections. We used as background files the blanck-sky fields provided in the CALDB data base that we reprocessed, reprojected and renormalized[2] to match observations. We detected point sources using the `wavdetect` tool and we extracted a light curve excluding them to identify and remove periods of enhanced background. We used the `fluximage` tool to produce images in the 0.7–2 keV bands and the appropriate exposure maps. We cleaned the images from point sources using `dmfilth` by replacing the count rates in the point source region with the mean value in a surrounding annulus. From the rescaled background files, we extracted images in the same energy band and with the same size of the cluster images that we use for background subtraction. As our analysis is based on flux measurements in the soft band and in the central regions of the clusters

---

[1] http://cxc.harvard.edu/ciao/threads/index.html

[2] We compute the renormalization factor as the ratio between the source and background count rate in the 9–12 keV band.

Table 1. Properties of the clusters in our Planck sample. Column (1) is the INDEX in the PSZ1 catalogue, column (2) the Planck name, column (3) provides an alternative name, columns (4) and (5) are the coordinates of the X-ray peak that we used to measure the concentration parameter, columns (6) and (7) are the redshift and mass as provided in the Planck catalogue, columns (8) and (9) are the concentration parameter and its error, while in column (10) we list the ID of the observations used in our analysis (those starting with '0' are *XMM–Newton* data). The full table is available online.

INDEX	NAME	Alt. name	$\mathrm{RA_X}$	$\mathrm{Dec._X}$	Redshift	M_{500} ($10^{14}\,\mathrm{M_{\odot}}$)	c	σ_c	Obs. ID
6	PSZ1 G002.77−56.16	RXC J2218.6−3853	22:18:39.66	−38:53:59.0	0.141	4.4	0.0585	0.0032	15101
10	PSZ1 G003.93−59.42	RXC J2234.5−3744	22:34:27.53	−37:43:57.0	0.150	6.6	0.0332	0.0016	15303
17	PSZ1 G006.45+50.56	RXC J1510.9+0543	15:10:56.09	+05:44:40.8	0.076	6.8	0.1701	0.0019	6101
18	PSZ1 G006.68−35.52	RXC J2034.7−3548	20:34:48.74	−35:50:54.6	0.089	4.0	0.0216	0.0017	12274
23	PSZ1 G008.33−64.74	ACO S 1077	22:58:48.32	−34:47:59.1	0.312	7.7	0.0478	0.0019	1562
24	PSZ1 G008.42−56.34	RXC J2217.7−3543	22:17:45.55	−35:43:22.4	0.148	4.8	0.0927	0.0050	15116
26	PSZ1 G009.02−81.22	RXC J0014.3−3023	00:14:19.04	−30:23:30.0	0.306	9.5	0.0223	0.0009	2212, 7915, 8477, 8557

(Section 3.3), where the source outshines the background, possible systematics in the background renormalization and subtraction do not affect significantly our results.

3.2 *XMM–Newton* data reduction

We reduced *XMM–Newton* observations with the SAS software 14.0 starting from the raw files in the archive, which we reprocessed to produce calibrated event files. We used the Extended Source Analysis Software (ESAS; Snowden et al. 2008) to filter periods affected by soft proton flares and to produce images in the 0.5–2.5 keV band for each detector. We also computed the appropriated exposure maps and a model image of the instrumental background for each detector. We then combined the images with the `comb` ESAS tool to produce EPIC images.

3.3 Measuring the concentration parameter

For each cluster in the PSZ1 and ME-MACS sample with available X-ray images, we computed the concentration parameter introduced by Santos et al. (2008):

$$c = \frac{F(r < 40\,\mathrm{kpc})}{F(r < 400\,\mathrm{kpc})}, \qquad (1)$$

where $F(r < 40$ kpc) is the flux within 40 kpc from the centre (representing the core region) and $F(r < 400\,\mathrm{kpc})$ is the flux within 400 kpc, representing the cluster emission. Santos et al. (2008) introduced this parameter to discriminate CC and NCC objects also at high redshift and using observations with poor statistics. They tuned the choice of the radii of the two regions (40 and 400 kpc) to separate more efficiently CC from NCC and to be able to compute c with *Chandra* data, both for their high-redshift sample ($z > 0.7$) and for intermediate redshift clusters ($0.1 < z < 0.3$). Since the clusters in our samples span a similar redshift range, we decided to use the original definition of the parameter that is furthermore the most used in the literature.

To compute the concentration parameter as in equation (1), we calculate the intensity of the cluster emission, using the background-subtracted and exposure-corrected *Chandra* or *XMM–Newton* images (Sections 3.1 and 3.2). We take into account the Poissonian noise in both source and background images and compute the error on the concentration parameter, which is typically of the order of 5 per cent. To define the two regions of interest, we need to fix a centre for the two circles and we decided to use the peak of the X-ray images, selected as the brightest pixels in the clean image after masking the point sources and smoothing it with a Gaussian with a full width at half-maximum (FWHM) of 7 arcsec to reduce statistical fluctuations. When multiple observations are available for the same object, we estimated the peak from the mosaic image to minimize the impact of statistical fluctuations especially for disturbed objects that do not feature a clear peak. We measured the total number of net counts and its error within 40 and 400 kpc, correcting for background, vignetting (through the exposure map) and CCD gaps when they intersect the regions of interest, and compute their ratio. When multiple observations are available for the same object, we measured the concentration parameter on each observation and compute their weighted mean. We tested that this procedure provides more consistent results than measuring the concentration parameter directly on the mosaic image. We applied the same procedure for the clusters in our PSZ1 sample and on the ME-MACS: we provide the estimated values in Tables 1 and 2.

Santos et al. (2010) show that for CC clusters the amount of *K*-correction is different for the inner 40 kpc, where the temperature is lower, than in the larger 400 kpc region and that this effect reduces the concentration parameter at high redshifts. They estimate that this effect will reach 15 per cent for strong CCs at $z = 1$, depending on the temperature in the inner region. As we do not have temperature profiles for all the clusters in our samples, we could not compute the correction factors directly for all objects. Nonetheless, we could estimate an upper limit to the intensity of this effect, by assuming for all CC clusters in our sample a minimum temperature of one-third of the virial temperature, which we estimated with the *M–T* scaling relation by Arnaud, Pointecouteau & Pratt (2005). We calculate the correction factor as described in Santos et al. (2010) and we find that the concentration parameters of CC clusters at a median $z = 0.25$ should be lower by $\simeq$5 per cent with respect to their values at $z = 0$. Given the limited redshift range of our samples and the high temperature of the intracluster medium (ICM) for massive clusters, this correction is thus comparable to or smaller than the statistical errors on the parameters. Nonetheless, comparison with samples or subsamples in different redshift ranges should be taken with caution.

4 RESULTS

4.1 The distribution in the Planck sample

In Fig. 2, we show the histogram of the concentration parameter distribution in the Planck sample with logarithmic bins. The distribution features a single peak at low values of the concentration parameters with a tail extending to higher values. The median concentration parameter is $c = 0.0475$.

We classified objects into two classes, CC and NCC, using a threshold value $c = 0.075$. This value is based on Santos et al.

Table 2. Properties of the clusters in the ME-MACS sample. Column (1) is the cluster name, columns (2) and (3) are the coordinates of the X-ray peak that we used to measure the concentration parameter, column (4) is the redshift of the clusters, column (5) is its mass calculated from the X-ray luminosity in Mann & Ebeling (2012), columns (6) and (7) are the concentration parameter and its error, while in column (8) we list the ID of the observations used in our analysis (those starting with '0' are *XMM–Newton* data). The full table is available online.

NAME	RA_X	$Dec._X$	Redshift	M_{500} (10^{14} M$_\odot$)	c	σ_c	Obs. ID
A1914	14:26:03.12	+37:49:24.9	0.17	8.08	0.0626	0.0014	3593
A209	01:31:52.76	−13:36:41.4	0.21	5.71	0.0482	0.0025	3579, 522
A586	07:32:20.61	+31:37:49.4	0.17	5.99	0.0835	0.0028	11723, 530
ABELL1689	13:11:29.52	−01:20:24.4	0.18	9.46	0.1188	0.0016	6930
ABELL1758	13:32:38.49	+50:33:35.0	0.28	5.41	0.0263	0.0016	2213
ABELL1835	14:01:02.10	+02:52:45.4	0.25	11.8	0.2500	0.0029	6880
ABELL2163	16:15:46.06	−06:09:06.0	0.21	12.3	0.0224	0.0006	1653
ABELL2204	16:32:46.94	+05:34:32.1	0.15	9.60	0.3051	0.0013	7940

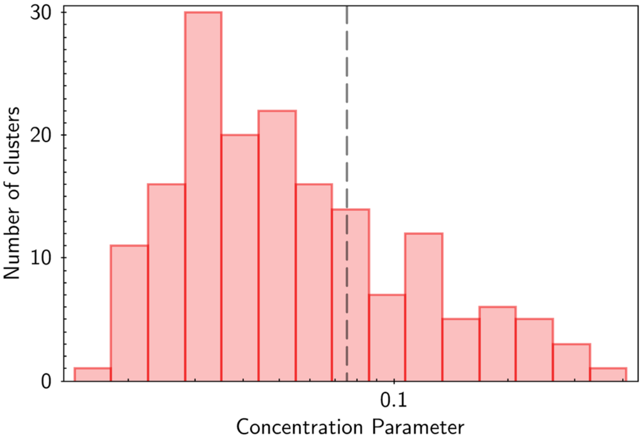

Figure 2. Distribution of the concentration parameter in the Planck sample. The vertical dashed line marks the threshold to separate CC ($c > 0.075$) from NCC ($c < 0.075$).

(2008), who calibrated it with the cooling time, to separate NCC and 'moderate CC'. We merged into a single CC class the 'moderate CC' and 'pronounced CC' classes of Santos et al. (2008). With this classification, we find 49/169 CC in our sample, corresponding to a CC fraction of (29 ± 3) per cent, where we estimated the error with bootstrap resampling. If we consider only the subsample with $z > 0.15$, we find a consistent value (29 ± 4) per cent.

As discussed in Section 2.1, our Planck sample is not fully complete and we are missing 20 objects from the original Planck cosmology sample. Even in the unlikely case that all missing clusters are classified as CC, the CC fraction of the Planck sample would rise only up to 36 per cent.

We divided the sample in redshift and mass subsamples to test for a possible evolution or mass dependence of the CC fraction, as measured by our indicator. The CC fractions for each subsample are shown in Table 3. We do not find a significant variation of the CC fraction with redshift in the PSZ1 sample. However, this is not in contrast with the results found by McDonald et al. (2013), who showed a significant evolution of the CC fraction, as measured by the concentration parameter, in their sample drawn from the SPT SZ catalogue. In fact, the evolution in the SPT sample becomes evident only in redshift bins at $z > 0.3$, a redshift range where we have only 24 objects in our Planck sample. Indeed, at $z > 0.3$, we could measure a CC fraction of 29 per cent with an error of 9 per cent, which does not allow us to draw any conclusion. Moreover, as discussed in Section 3.3, we could not apply the K-correction to our data set and this prevents us from deriving strong constraints on the evolution of the CC fraction.

Table 3. CC fraction in redshift and mass subsamples of the Planck sample.

Subsample	CC fraction (per cent)
$z < 0.18$ (median)	27 ± 5
$z > 0.18$ (median)	30 ± 5
$z > 0.15$ (ME-MACS)	29 ± 4
$M < 6.5 \times 10^{14}$ M$_\odot$	24 ± 4
$M > 6.5 \times 10^{14}$ M$_\odot$	34 ± 5

Concerning the mass dependence, we see a small difference in the CC fraction, with the low-mass subsample featuring a lower CC fraction than the high-mass subsample. Although this result is likely a statistical fluctuation (1.5σ), it is interesting to note that a similar behaviour has been found also by Mantz et al. (2015): using their SPT sample, they find a higher fraction of 'peaky' objects among hotter clusters, while they do not find a similar trend for X-ray-selected samples. The opposite trend has in fact been noted in X-ray surveys, where low-mass objects are predominantly CC (e.g. Chen et al. 2007), possibly as a consequence of the CC bias (see discussion in Eckert et al. 2011). Nonetheless, an increasing CC fraction with mass is not expected and, under the hypothesis that CCs are relaxed systems, seems to contradict the prediction of hydrodynamical simulations that find an increasing fraction of merging clusters as a function of mass (Fakhouri, Ma & Boylan-Kolchin 2010). We underline that this trend is poorly significant in both the Planck and SPT samples and needs to be verified with a larger number of objects, possibly SZ selected.

4.2 Comparison with ME-MACS

In Fig. 3, we compare the distribution of the concentration parameter of the Planck sample (described in Section 4.1) with the one in the ME-MACS sample. The distribution of the X-ray-selected ME-MACS is qualitatively different from the one of the Planck sample: it shows two peaks, one for the NCC objects and one corresponding to CCs.

Most objects in ME-MACS are classified as CC and the CC fraction is 59 ± 5 per cent. We can compare it directly with the CC fraction in the Planck sample estimated with the same indicator and the same threshold (Section 4.1): the difference is significant at more

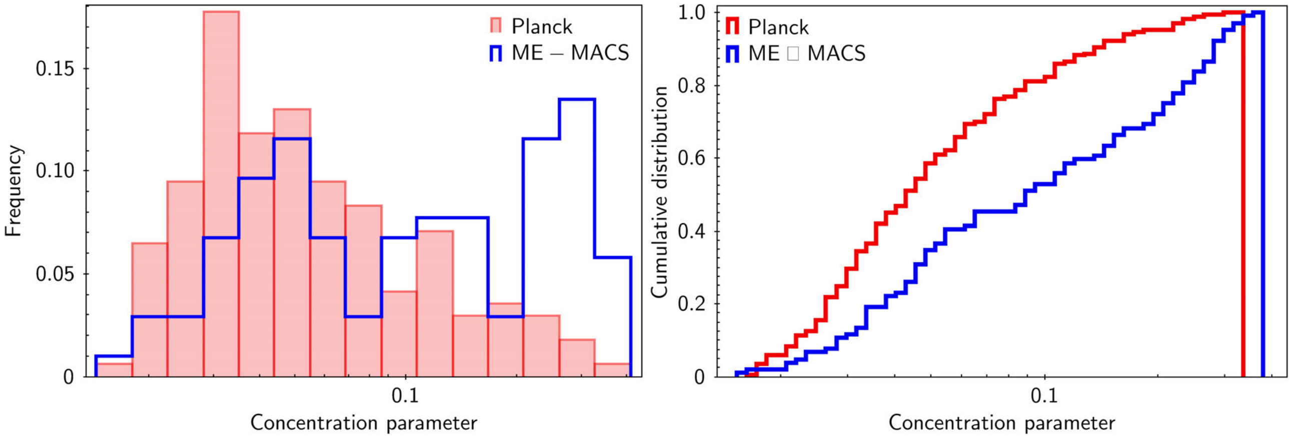

Figure 3. Histogram (left) and cumulative (right) distribution of the Planck (red) and ME-MACS (blue) samples.

than 5σ. The difference is still significant even when compared to the CC fraction in the Planck subsample with $z > 0.15$ (29 ± 4 per cent). Even assuming that all the clusters that meet the ME-MACS criteria but do not have *Chandra* observations (Section 2.2) are NCC, the CC fraction would decrease only to 47 per cent, larger at 3σ than the fraction in the Planck sample.

We can further apply statistical tests to compare the two distributions shown in Fig. 3 to assess that they are different independently of the choice of the threshold separating CC from NCC. We use the Kolmogorov–Smirnov (KS) test, which measures the probability that the two samples are drawn from the same parent distribution. The KS statistic D, that is the supremum distance from the two cumulative distributions (Fig. 3), is 0.349, with a null-hypothesis probability $p_0 = 1.68 \times 10^{-7}$, showing that the Planck and ME-MACS distributions are significantly different. If we consider only the Planck subsample with $z > 0.15$ (Section 2.3), the KS still returns a significant difference between the Planck and ME-MACS samples ($D = 0.334$ and $p_0 = 1.24 \times 10^{-5}$).

The result of the KS test is supported by the qualitative difference between the two distributions: two peaks seem present in the ME-MACS sample, whereas the distribution of Planck values looks more consistent with a peaked distribution with a tail at high-concentration values, that is a positively skewed function. We tested these differences quantitatively performing a maximum likelihood fit for each of the two distributions on the unbinned data using the MCLUST package (Fraley & Raftery 2002; Fraley et al. 2012) and the FITDISTR function of the package MASS (Venables & Ripley 2002) in the software environment R version 3.2.2 (R Core Team 2015). The model-based clustering implemented in MCLUST is an algorithm for fitting normal mixture models; that is, maximum likelihood fits are performed assuming a number from 1 to 9 normal components are present in the data. The function FITDISTR performs a maximum likelihood fit of the data to some probability distribution functions, either calculated using analytic formulae (as e.g. in the lognormal case) or computed by optimization of the likelihood. We chose for fitting two commonly used positively skewed functions: the Weibull and lognormal distributions. We performed model selection comparing the Bayesian information criterion (BIC; Schwarz 1978) defined as $\mathrm{BIC} = 2\ln L - k\log(n)$, where L is the likelihood, k is the number of parameters of the model and n is the number of data points; $k\log(n)$ is the penalty term that compensates the difference in likelihood due to an increase in the number of fitting parameters. The best model is the one that maximizes the BIC. Commonly adopted thresholds for the difference in BIC values of two models are: a BIC difference of 0–2 is considered as weak evidence, 2–6 as positive evidence, 6–10 as strong evidence and >10 as very strong evidence in favour of the model with the greater BIC value (Kass & Raftery 1995; Raftery 1995). We did not work on log space because the positively skewed functions are not defined for negative values. For ME-MACS, the result of the normal mixture model strongly disfavours a single Gaussian component, with a BIC value of 159.88 with respect to two Gaussian components with a BIC value of 217.99. A three-component Gaussian model has a BIC value of 219.88 so the improvement is not significant. The two components consist of 41 and 62 members with the separation at a value of 0.07 (see Fig. 4, left-hand panel), which is similar to the threshold to separate CC and NCC that we adopted in our analysis. The fit with positively skewed functions returns BIC values of 203.70 and 202.23 for the lognormal and Weibull distributions, respectively. Those models are therefore clearly disfavoured with respect to a two-component normal mixture model.

For the Planck sample, the model with the highest BIC value is the one with three Gaussian components, with a BIC value of 610.20 that is significant with respect to a two-component model that has a BIC value of 597.63. The optimal partition returns three groups with 71, 59 and 39 members, respectively, with separations at values of the concentration parameters of 0.04 and 0.09 (see Fig. 5, left-hand panel). The fit with a lognormal function returns a BIC value of 622.60 so this model is favoured with strong evidence with respect to the best three-component normal mixture model. A Weibull distribution is also disfavoured as its BIC value is 572.82. We can therefore conclude that the distribution of concentration parameters of the Planck sample is described by a lognormal distribution, while the ME-MACS catalogue is best described by a bimodal behaviour. The secondary peak at high-concentration parameter in the latter distribution may be due to the CC bias, as the number of peaked objects is artificially boosted in X-ray surveys (Section 5.2).

We tested the correlation between the concentration parameter and the dynamical indicator that we used in Paper I (i.e. the projected distance between the X-ray peak and the brightest cluster galaxy) and found them to be significantly anticorrelated in both samples. We provide the details of this analysis in Appendix A.

4.3 Comparison with other samples in the literature

As discussed in Paper I, ME-MACS is the most suited sample to be compared with Planck among the well-defined X-ray-selected

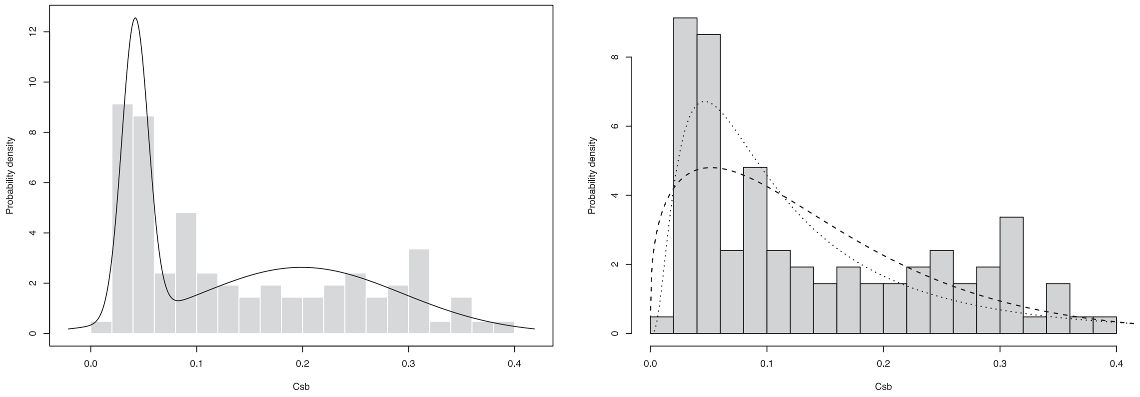

Figure 4. Left: the distribution of concentration parameters for the ME-MACS sample with the best-fitting model with two gaussian components overplotted. Right: same as in the left-hand panel with the fit positively skewed functions: with the dotted line a lognormal and with the dashed line the Weibull function.

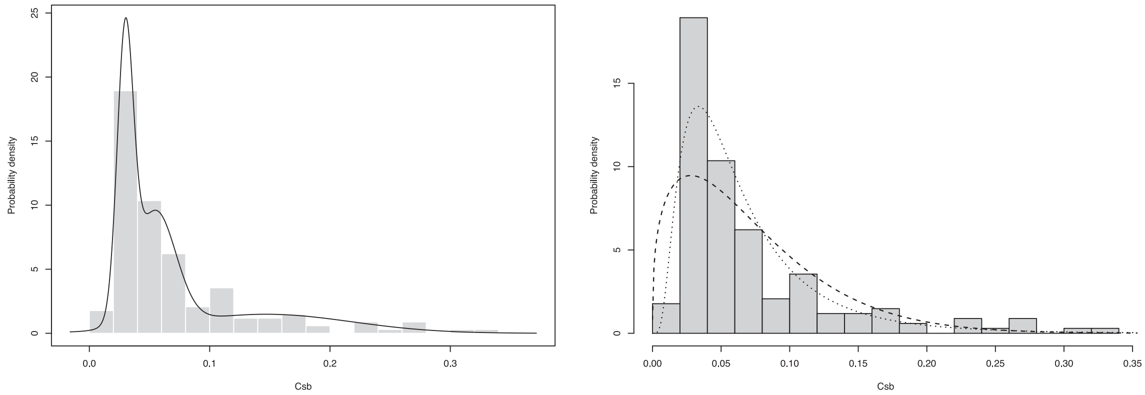

Figure 5. Left: the distribution of concentration parameters for the Planck sample with the best-fitting model with three gaussian components overplotted. Right: same as in the left-hand panel with the fit positively skewed functions: with the dotted line a lognormal and with the dashed line the Weibull function.

Table 4. CC fraction in literature samples and KS test compared with the Planck sample.

Sample	CC fraction (per cent)	KS test $D\,(p_0)$	Median z	Median M_{500} ($10^{14}\,\mathrm{M_\odot}$)	Number of objects
Planck	29 ± 4	–	0.18	6.2	169
Planck $z > 0.15$	29 ± 5	–	0.25	7.08	103
ME-MACS	59 ± 5	0.349 (1.7×10^{-7})	0.35	6.54	129
HIFLUGCS (X)	56 ± 6	0.316 (1.3×10^{-4})	0.047	2.70	62
V09 low-z (X)	58 ± 10	0.334 (9.0×10^{-3})	0.075	6.18	26
V09 high-z /400d (X)	31 ± 8	0.147 (5.5×10^{-1})	0.49	2.90	36
Pascut15 (X)	74 ± 5	0.471 (1.5×10^{-9})	0.50	2.72	62
Santos10 (X)	60 ± 13	0.421 (1.0×10^{-2})	0.82	2.18	15
SPT all (SZ)	29 ± 5	0.192 (3.0×10^{-2})	0.59	5.17	81
SPT low-z (SZ)	29 ± 7	0.170 (2.7×10^{-1})	0.47	5.60	41

catalogues we used in that paper, and this is the reason we focused our analysis on it in this paper. Nonetheless, the concentration parameter has been calculated for many other samples of galaxy clusters with the definition of Santos et al. (2008) and we can use the tabulated values for calculating their CC fraction and for doing a KS test to compare with the Planck sample. We found literature information on the concentration parameter for HIFLUGCS (Hudson et al. 2010; T. Reiprich private communication), the *Chandra* Deep Group survey in Pascut & Ponman (2015), a high-redshift sample computed by Santos et al. (2010) and built using WARPS (Perlman et al. 2002; Horner et al. 2008) and RDCS (Rosati et al. 1998), and the two samples used in the cosmological analysis by Vikhlinin et al. (2009): the low-z one, whose c values are provided by Santos et al. 2010, and the high-z subsample, drawn by 400d (Burenin et al. 2007), for which the c values were computed by Semler et al. (2012). We note that the above samples span different masses and redshift ranges (as shown in Table 4) since they are derived with different limiting fluxes starting from X-ray surveys, based either on RASS (HIFLUGCS, ME-MACS) or on deep pointed ROSAT observations (400d, WARPS and RDCS). We also found tabulated value of the concentration parameter for the SZ-selected SPT XVP sample, described in McDonald et al. (2013). The CC fraction (using the same threshold value $c = 0.075$), the results of the KS test in comparison with our Planck sample and the median redshift and mass of each sample are provided in Table 4.

This analysis confirms that the ME-MACS sample is the most similar in terms of both mass and redshift to the Planck sample. The CC fractions of most X-ray-selected samples are significantly higher than those in Planck in all redshift and mass ranges, with the notable exception of the high-redshift sample of Vikhlinin et al. (2009), drawn from 400d, which features a fraction consistent with Planck. The difference between this sample and other X-ray-selected samples has been already debated in the literature (e.g. Santos et al. 2010; Mantz et al. 2015), and it is beyond the scope of this paper. Nonetheless, we notice that the limiting flux of 400d (1.4×10^{-13} erg cm^{-2} s^{-1}; Burenin et al. 2007) is higher than those of WARPS (6.5×10^{-14} erg cm^{-2} s^{-1}) and RDCS ($1 - 3 \times 10^{-14}$ erg cm^{-2} s^{-1}), which are also based on deep *ROSAT* pointed observations. Possibly, the higher flux threshold imposed in 400d with respect to the detection limit reduces the effect of the CC bias (Eckert et al. 2011; Rosati et al. 2002) and allows us to build a 'representative snapshot of the cluster population of typical clusters at $z = 0.3$–0.8' (Burenin et al. 2007). We also note that the difference in the CC fraction of RDCS+WARPS sample and 400d discussed by Santos et al. (2010) is due to the difference in limiting fluxes cited above: all the CC objects in RDCS or WARPS have a measured flux below the 400d threshold. Given that 400d is the only X-ray sample featuring a CC fraction consistent with Planck, it is not surprising that Semler et al. (2012) and Nurgaliev et al. (2016) found that the distribution of concentration parameters and of morphological indicators is consistent in SPT-selected samples and 400d. However, it appears clear that 400d is rather unique among X-ray samples.

The only other SZ-selected sample in Table 4 is SPT XVP (McDonald et al. 2013), which features a CC fraction consistent with the one in Planck. Since the SPT-XVP sample extends to higher redshift (0.32–1.2) and lower masses than the Planck sample, we extracted a subset from the SPT catalogue in the redshift range 0.32–0.6 (41 objects) and compare it with the Planck sample in the same redshift range (only 24 clusters). The CC fraction is in very good agreement as SPT finds 29 ± 7 per cent, while with the Planck subsample we have 29 ± 9 per cent. It is certainly intriguing that both SZ-selected samples provide a similar CC fraction, but the large error bars, due to the limited number of objects in the common redshift range, do not allow us to draw strong conclusions about this agreement of the CC fraction in different SZ-selected samples.

5 THE ROLE OF CC BIAS

In this section, we test the hypothesis that the difference between the Planck and ME-MACS distributions of concentration parameters is due to the CC bias, first by looking at the properties of clusters that are detected only in ME-MACS and not in Planck (Section 5.1) and then by performing dedicated simulations (Section 5.2).

5.1 Missing ME-MACS clusters in Planck

In Fig. 1, we show the distribution of Planck and ME-MACS objects in the mass–redshift plane: the mass limit of the ME-MACS sample is below the one of our Planck sample in the redshift range 0.2–0.6. Therefore, we expect to find in the Planck sample only the most massive ME-MACS objects, which we selected for having $M_{500} > 8 \times 10^{14}\,\mathrm{M}_{\odot}$ at $z > 0.4$ or $M_{500} > 7 \times 10^{14}\,\mathrm{M}_{\odot}$ in the redshift range 0.15–0.4. We found 36 objects in ME-MACS with the above criteria and 24 are in common with Planck while 12 are not found in our Planck sample. Of these, three are located behind the galactic mask and we are thus left with nine massive objects that should be found also in the Planck sample but are not. We looked at their concentration parameters and all of them are classified as CCs. It is interesting to note that most of the 'missing clusters' in our Planck sample feature a strongly peaked SB profile ($c > 0.2$) and belong to the secondary peak of the ME-MACS distribution, which is not found in the Planck histogram (Section 4.2).

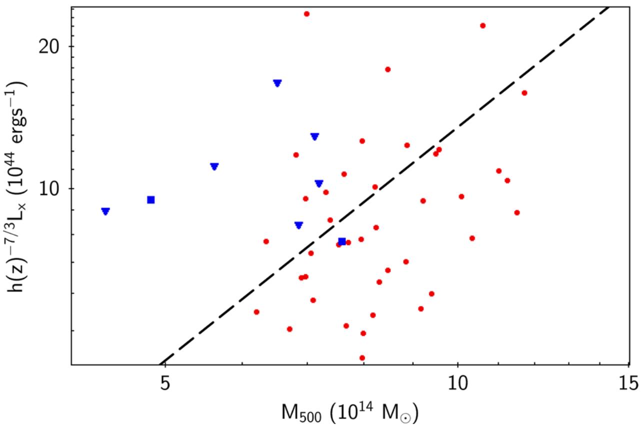

Figure 6. Distribution in the *L–M* plane of the clusters in common between Planck and ME-MACS (filled red circles) and for those in ME-MACS but not in Planck (blue triangles for SZ-derived mass measurement and blue square for weak lensing). The dashed line marks the scaling relation of Pratt et al. (2009).

We underline that the masses of ME-MACS that we used to select potential Planck clusters are calculated from the *L–M* scaling relation (see Section 2.3) and may thus be biased high for CCs (e.g. Hudson et al. 2010). For eight of the missing objects, we found independent mass measurements, either in the Planck catalogue (Planck Collaboration XXIX 2014, i.e. they are detected by Planck with an S/N in the range 4.5–7 and thus do not enter in the cosmology sample that we analysed here) or from weak lensing (for two of them) in the LC^2 catalogue (Sereno 2015). We show their position in the *L–M* plane along with the common objects in the two samples in Fig. 6. Almost all the missing objects lie above the scaling relation and their independent mass measurements are below the mass limit of our Planck sample, explaining why they are not found in the Planck cosmology sample. Their luminosity (and thus their mass estimate from *L–M*) is likely boosted by the presence of the CC.

The fact that all the objects we considered here are CC suggests that the CC bias may have a role in explaining the difference between the two samples. However, to firmly test this hypothesis observationally, one would need to start from a complete population of clusters with independent mass measurements and to compare it with the properties of SZ-selected and X-ray-selected samples with similar mass limits, to see which clusters are missing in the two samples. Unfortunately, we are not in this situation, since the ME-MACS mass limit is below the Planck one and the mass measurements of ME-MACS are derived from a biased quantity such as the luminosity. To firmly test the effect of CC bias, we thus need to make use of numerical simulations (Section 5.2).

5.2 Simulations

We performed a dedicated simulation following an approach similar to Eckert et al. (2011) and tailored to reproduce the Planck and ME-MACS selection criteria. The main idea of the procedure is to simulate a realistic population of clusters in the mass–redshift plane with a distribution of concentration parameters, that follows the one in the Planck sample, apply the ME-MACS selection function to the simulated systems and measure the CC fraction in the ‘detected’ simulated sample. We refer to Eckert et al. (2011) for the details of the simulation; here we recall the main steps and discuss the differences with respect to the previous approach.

We start by simulating a population of haloes in the appropriate mass and redshift range. As opposed to Eckert et al. (2011), who started from an X-ray luminosity function tailored for their sample, here we randomly draw haloes according to the mass function of Tinker et al. (2008). We then use the relation between core-excised X-ray luminosity and halo mass of Mantz et al. (2010) to calculate the expected luminosity of each halo.

To convert the core-excised luminosity into an integrated luminosity and overall flux, we associate a surface brightness profile to each simulated cluster. We underline that this is an improvement with respect to Eckert et al. (2011), because we take into account that at a fixed mass, CC clusters are actually more luminous than NCC clusters (see discussion in Hudson et al. 2010). In the original simulation, Eckert et al. (2011) used a fixed surface brightness template (a beta model for NCC and a double-beta model for CC) and randomly chose between the two according to a fixed input CC fraction. Here, we assume that the distribution of the concentration parameters of the Planck sample is representative of the true distribution and we use the full measured distribution to draw a realistic distribution of surface brightness profiles. We assume that the surface brightness profile of each cluster can be approximated by a double-beta model:

$$S(r) = S_1 \left(\left[1 + \left(\frac{r}{r_{c1}} \right)^2 \right]^{-3\beta+1/2} + R \left[1 + \left(\frac{r}{r_{c2}} \right)^2 \right]^{-3\beta+1/2} \right), \tag{2}$$

where the ratio between the two beta models, R, is randomly selected from a list of values that reproduce the c distribution of the Planck sample, while β, r_{c1} and r_{c2} are fixed to the values that best represent the observed values in the Planck sample ($\beta = 0.64$, $r_1 = 300$ kpc, $r_2 = 30$ kpc) and S_1 is the overall normalization, which is set on the fly to reproduce the core-excised luminosity of each simulated halo. This approach allows us to simulate a population spanning a whole range of surface brightness profiles, but the results do not change significantly if a fixed template is used. After having selected a surface brightness profile, we can reproduce the integrated luminosity and the flux in the 0.1–2.4 keV energy range for each simulated cluster, as described in Eckert et al. (2011). A hidden assumption in this procedure is that the Planck distribution of concentration parameter is representative of the cluster population at all redshifts, that is, that the CC fraction does not evolve with time, in contrast with the recent result by McDonald et al. (2013). However, this evolution becomes strongly significant only at very high redshift ($z > 0.7$), where we have very few objects both in our simulations and in the observed samples.

We then simulate the ME-MACS selection. As described in Mann & Ebeling (2012), the starting point of the ME-MACS (and also MACS; Ebeling et al. 2001) is the RASS Bright Source Catalogue (Voges et al. 1999), from which they selected candidate clusters with a flux limit $f_{\rm RASS} > 10^{-12}$ erg cm^{-2} s^{-1}. We can thus use the same procedure as in Eckert et al. (2011) to simulate the source detection as ME-MACS is a RASS-based flux-limited survey. We only apply the additional luminosity and redshift criteria in ME-MACS, namely $L_{\rm X} > 5 \times 10^{44}$ erg s^{-1} and $z > 0.15$.

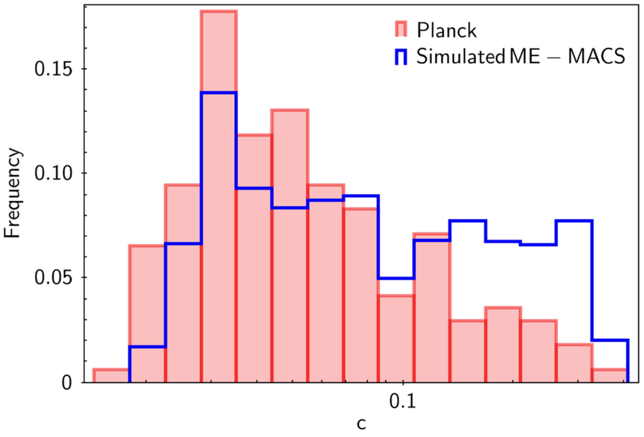

Figure 7. Distribution of the concentration parameter in the Planck sample (pink), used as an input in the simulation, and the output distribution of concentration parameters of the detected clusters in the ME-MACS simulation (blue). The vertical dashed line marks the threshold to separate CC ($c > 0.075$) from NCC ($c < 0.075$).

We run our simulation with 10^7 input haloes, resulting in more than 15 000 detected clusters, for which we compute the concentration parameter. We compare the c output distribution with the input one in Fig. 7: it is apparent that a second peak of the distribution emerges at high-concentration parameters (i.e. CC). While the starting population is described by the Planck lognormal distribution, the output of the simulation is not described by a unimodal distribution anymore and a secondary peak emerges. Our simulation thus shows that the ‘bimodality’ (i.e. presence of two peaks) of the cluster population between CC and NCC objects, which has been largely discussed in the literature (e.g. Cavagnolo et al. 2009; Pratt et al. 2010), is at least partly due to the CC bias.

The CC fraction in the whole simulated sample is 48 per cent, significantly larger than the fraction in the Planck sample, but still lower than the measured value of the ME-MACS sample (59 ± 5 per cent). Since the Planck and ME-MACS samples largely overlap and are drawn from the same underlying population, there is a strong covariance between the CC fractions measured in the two samples. This covariance needs to be taken into account to assess the significance of the difference between the two samples. To this aim, we perform another set of simulations in which the number of simulated haloes reproduces the expected number of haloes in the redshift and mass range of interest. We then apply at the same time the Planck and ME-MACS selection functions to the simulated haloes to draw realistic Planck-like and ME-MACS-like cluster samples simultaneously and calculate the CC fraction in both. To implement the Planck selection function, which is given as a function of the total SZ flux (Y) and the apparent opening angle (Planck Collaboration XXVII 2016), we use the Y–M relation from Planck Collaboration XX (2014). We then repeat this procedure 10 000 times and compare the resulting CC bias values with the observed one. In Fig. 8, we show the 68.3 and 99.7 per cent containment contours of the output values for the CC fraction. The figure clearly shows the strong covariance between the two measurements, which results from the fact that the two samples are not independent. In only 0.2 per cent of the cases, we are finding that the two CC fractions are consistent with the observed ones simultaneously.

To summarize, our simulation reproduces qualitatively the properties of the ME-MACS sample and the presence of two peaks. It shows that the CC bias certainly plays a large role in the difference

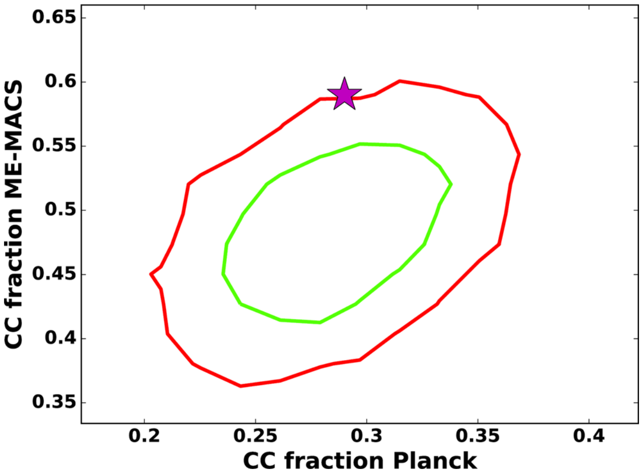

Figure 8. Probability contours of the CC fraction drawn from 10 000 simulated populations of massive clusters, applying the Planck and ME-MACS selection functions to the simulated data. The contours represent a containment of 68.3 per cent (red) and 99.7 per cent (green) of the simulations. The magenta star shows the true Planck and ME-MACS CC fractions.

between the Planck and ME-MACS distributions, but at the same time suggests that it is unlikely that CC bias alone can account for the full difference. However, we should remind that our attempt to reproduce the effect of the CC bias, although sophisticated, is based on several assumptions and, as any simulation, cannot fully reproduce the complexity of the clusters population and of the X-ray and SZ selection. Moreover, as our samples are not fully complete, there is still the possibility that the difference may be fully explained by the CC bias, if we assume that the 12 missing clusters in the Planck $z > 0.15$ sample (Section 2.1) are CC (rising the CC fraction to 36 per cent) and all unobserved objects in ME-MACS (25; Section 2.2) are NCC (lowering it to 47 per cent). Although we consider this hypothesis unlikely, we cannot exclude it, given the incompleteness of our sample.

6 BEYOND THE CC BIAS

In Section 5, we focused our attention on the role of CC bias in explaining the difference between the Planck and ME-MACS distributions. However, there are other mechanisms, both in the SZ and in the X-ray selection, that can contribute to the difference and that can be highlighted by the comparison of our samples. In this section, we discuss the role of possible biases against CCs in the *Planck* survey (Section 6.1) and the effect due to a population of X-ray underluminous objects (Section 6.2) in the Planck catalogue (Planck Collaboration XXVII 2016).

6.1 An anti-CC bias in the *Planck* SZ survey

It has been suggested that the presence of bright radio galaxies at the centres of CC clusters may induce a bias against CCs in SZ surveys, since radio sources could potentially influence the cluster detection and measurement of the SZ signal (e.g. Sayers et al. 2013a; Lin et al. 2015) and are thus usually masked out in the SZ analysis. As discussed in Planck Collaboration XXIX (2014), this bias is expected to be small in the *Planck* survey, as the cluster detection is performed at high frequencies, where the emission of steep-spectrum radio sources is negligible with respect to the SZ effect. Nonetheless, we tried to estimate this possible bias that could in principle contribute to the residual difference that we found in Section 5.2. The point source mask used in the Planck analysis was built starting from the Planck compact source catalogues (Planck Collaboration XXVIII 2014) at several frequencies, excluding a circle of radius 2.13 FWHM around point sources detected with S/N ratio larger than 10 (Planck Collaboration XXIX 2014). Starting from the Meta-Catalogue of X-ray-detected Clusters (MCXC; Piffaretti et al. 2011), we looked for known clusters whose position is within a radius of 2.13 FWHM around bright point sources in at least one out of the six HFI frequencies, finding 57 candidate 'missing' clusters. However, most of these objects have low masses and should not be detectable by *Planck*. Only for six objects (namely Perseus, Cygnus A, Abell 780, RXC J1130.3 − 1434, RXC J1025.9 + 1241, Abell S1111), the masses in the MCXC catalogue are comparable with the masses of clusters in the PSZ1-cosmo sample at the same redshift and they could thus be detected in the survey if they were not behind the mask. Perseus, Cygnus-A and Abell 780 are well-known CC clusters, while we could not find any literature information about the core state of the remaining three objects, whose expected mass is furthermore close to the limit of the selection function in the mass–redshift plane and may thus be not detected by *Planck*, also for statistical reasons. We can thus roughly estimate that the Planck catalogue is missing 3–6 objects because of radio sources, and assuming that they are all CC, the corrected CC fraction would be 30–31 per cent. The bias due to radio galaxies in CC is thus only 1–2 per cent, smaller than the statistical error on the CC fraction in the Planck sample, and not sufficient to reach the CC fraction of 38 per cent that would be needed to reproduce the ME-MACS fraction with our simulation of the CC bias.

Another possible reason for which the *Planck* SZ survey may be biased against CC is that through the SZ effect we may in principle detect more easily disturbed merging clusters, where the SZ signal may be enhanced by shock fronts propagating in the ICM. Indeed, Sommer & Basu (2014) showed that the SZ signal within R_{500} in simulated clusters is boosted after a merger on a time-scale of a few Gyr. The selection function and its dependence on the dynamical state of the *Planck* SZ survey have been tested in Planck Collaboration XXVII (2016) with Monte Carlo simulations, by injecting simulated clusters with different y maps in the *Planck* sky maps and running the detection algorithms, showing that the cluster morphology does not impact significantly the source detection. This result is not unexpected if we take into account the large beams of the Planck frequency channels: similarly to what happens to the peaked pressure profile of CC clusters, overpressurized regions due to shocks are smoothed out by the Planck moderate spatial resolution. Moreover, Planck is more sensitive to the behaviour of the pressure profiles at large scales than to the smaller scale physics (such as CCs or shock) and it measures the SZ signal on scales larger than R_{500} (i.e. the region studied by Sommer & Basu 2014).

Recently, Nurgaliev et al. (2016) suggested that Planck may be more sensitive to pairs or triplets of galaxy clusters, because of its large beam capturing an inflated signal from multiple objects and therefore may be biased towards merging systems. While it is certainly true that *Planck* has detected a few of these objects that received a lot of attention in the literature (Planck Collaboration IX 2011; Planck Collaboration VI 2013), in the high purity PSZ1 cosmology sample that we analysed in this paper and in Paper I, we do not have a large number of these objects. Moreover, clusters in multiple systems are not necessarily disturbed NCC objects: for instance, the brightest member in the *Planck* discovered supercluster

PLCK G214.6 + 37.0 features a prominent surface brightness peak associated with the BCG (Planck Collaboration VI 2013), which would lead us to classify it as a CC relaxed object.

Last but not least, if there were a systematic difference between the pressure profile of CC and NCC clusters at $R \gtrsim R_{500}$, with NCC clusters showing flatter profile than CC clusters similarly to what observed in the gas density distribution (Eckert et al. 2012), NCC could possibly have a larger SZ signal at large scales making them easier to detect in SZ. However, the analysis of the pressure profiles of samples of galaxy clusters both with *Planck* (Planck Collaboration V 2013) and with Bolocam (Sayers et al. 2013b) shows only a moderate difference at large scales and with a large dispersion. Indeed, if we assume the best-fitting models for CC and NCC objects in the analysis of Planck pressure profiles (Planck Collaboration V 2013) and we integrate them to measure the SZ signal at $5\,R_{500}$, the derived values differ only by 2 per cent. Nonetheless, the SZ flux at $5\,R_{500}$ strongly depends on the shape of the pressure profile: if we assume a combination of parameters consistent at 68 per cent with the best-fitting model but with a flatter outer slope $\beta = 3.2$ (basing on fig. 5 in Planck Collaboration V 2013), the derived $Y_{5\,R_{500}}$ would be 12 per cent larger than the value with the mean CC profile. We underline that the sample of clusters for which the Planck pressure profile has been measured is not SZ selected, as it is composed of early *Planck* detections already known in X-rays and with available *XMM–Newton* data (Planck Collaboration V 2013), thus the derived pressure profile may not be representative of the cluster population. While the present data do not allow us to provide support to the hypothesis of an anti-CC bias in Planck, more detailed studies on larger and well-defined samples are needed to reduce the uncertainties and to firmly assess the shape of the CC and NCC pressure profiles and their role on the SZ detection procedures.

6.2 X-ray underluminous clusters

One unexpected result of the *Planck* SZ survey has been the discovery of a population of X-ray underluminous clusters (Planck Collaboration XXVII 2016). These systems feature an X-ray luminosity that is well below the value that could be expected through scaling relations from the SZ signal, while their optical richness is in agreement with expectations. This population was highlighted at low redshift and in the Sloan Digital Sky Survey sky area, but it possibly extends also to other redshift ranges and sky regions. If this population exists also in our Planck sample and if all, or most, underluminous clusters are classified as NCC, it could contribute in explaining the difference between the CC fraction in the Planck sample and in ME-MACS. As these objects by definition obey a different *L–M* scaling relation than the one we used in Section 5.2, their presence is not accounted for in our simulation.

One method to highlight this population in our Planck sample is to look at the clusters that should have been detected also in ME-MACS but are not (complementary to what we showed in Section 5.1). We thus select all clusters in the Planck sample, which lie in the sky region covered by ME-MACS, have $z > 0.15$ and an expected luminosity larger than the ME-MACS threshold (see Mann & Ebeling 2012 for details) but are missing in the ME–MACS sample. To estimate the expected luminosity, we convert the SZ signal Y_{500} in the Planck catalogue into L_{500}, using the L_{500}–Y_{500} relation obtained in Planck Collaboration XXVII (2016). With this method, we find 24 missing clusters in ME-MACS, most of which (19) are NCC objects. In Fig. 9, we compare their measured luminosity[3] L_{500} as a function of their SZ signal, with the scaling relation and its scatter, calibrated on Planck clusters by Planck Collaboration XXVII (2016). We notice that almost all objects lie below the expected relation and some of them below twice the intrinsic scatter, which would lead to their classification as ‘underluminous’ objects, following Planck Collaboration XXVII (2016). According to the concentration parameter, all the most deviant objects are classified as NCC. We noticed that in a few cases the measured luminosity is above the selection threshold of the ME-MACS sample (5×10^{44} erg s^{-1}). However, we used luminosities within R_{500}, while the luminosity used in the selection of the ME-MACS sample is estimated in the RASS detection cell. Indeed, one of the most luminous clusters in Fig. 9 is A115N, which has $L_{500} = 7.5 \times 10^{44}$ erg s^{-1} in MCXC, but with $L_{\rm RASS,det} = 4.4 \times 10^{44}$ erg s^{-1} it fails to make the luminosity cut in ME-MACS (H. Ebeling, private communication).

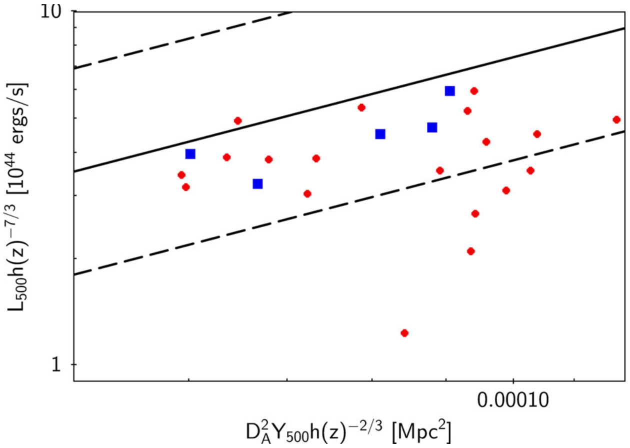

Figure 9. Distribution in the Y_{500}–L_{500} plane of the 24 missing ME-MACS clusters, compared with the best-fitting scaling relation (black continuous line) and its dispersion (±2σ, dashed lines) estimated in Planck Collaboration XXVII (2016). We mark with blue squares CC clusters and with red points NCC.

The population of X-ray underluminous clusters is thus likely present also in the Planck sample we are analysing. It is intriguing that candidate X-ray underluminous clusters in our sample are almost all classified as NCC: if this population, which is missing in X-ray surveys but is detected in SZ, is composed of disturbed NCC clusters, they could certainly contribute to the residual difference between the Planck and ME-MACS distributions of concentration parameters. At the moment, little is known about these objects, and it is unclear if they are truly X-ray underluminous for their mass or if their SZ signal is artificially boosted. New observations, both in X-rays and possibly in SZ, are needed to assess the origin of this class of objects. A systematic analysis of their properties and the CC state of X-ray underluminous clusters is beyond the scope of this paper and will be presented in a forthcoming work with new dedicated data (Rossetti et al., in preparation).

7 SUMMARY AND CONCLUSIONS

In this paper, we studied the CC state of an SZ-selected sample of galaxy clusters, the cosmological sample of the first Planck SZ

---

[3] For most objects, we used the luminosity in the MCXC catalogue (Piffaretti et al. 2011), while for five objects we measured the luminosity directly from the *Chandra* data.

catalogue (Planck Collaboration XXIX 2014), using as an indicator the concentration parameter (Santos et al. 2008). Our results are summarized as follows.

(i) The distribution of the concentration parameters in the Planck sample features a single peak at low values of c. The fraction of CC clusters ($c > 0.075$) is (29 ± 4) per cent.

(ii) We do not find indications of evolution of the CC fraction by dividing our sample in two redshift bins. Our result does not contradict previous detections that report evolution in a redshift range ($z > 0.3$), which is poorly sampled by our catalogue (McDonald et al. 2013). We find an indication of a larger CC fraction in higher mass systems, as reported also in Mantz et al. (2015), but only at low significance (1.5σ).

(iii) We compared the distribution of the concentration parameter with the one of the X-ray-selected ME-MACS sample (Mann & Ebeling 2012). The distributions are significantly different with a 1.7×10^{-7} probability that they are drawn from the same population of objects. Indeed, ME-MACS hosts a much larger fraction of CC objects: (59 ± 5) per cent.

(iv) The distribution of concentration parameters in ME-MACS shows two peaks and is well described by two Gaussians. This double-peaked distribution, which is observed also in other X-ray-selected samples and with other CC indicators (Cavagnolo et al. 2009; Pratt et al. 2010), has opened a debate in the literature whether the cluster population is bimodal or not. However, our Planck sample is better described by a single lognormal distribution. We showed with simulations that a secondary peak at high-concentration parameters emerges in X-ray flux-limited samples as a consequence of the CC bias and the presence of two peaks may thus not be an intrinsic property of the cluster population.

(v) Among the X-ray-selected samples available in the literature, ME-MACS is the one with the mass and redshift distributions more similar to the Planck sample (Paper I). Nonetheless, we compared the c distribution in Planck with the one of other X-ray samples and found them to be significantly different, having CC fractions in the range 56–74 per cent. We also compared our distribution with the one in the SZ-selected sample of SPT clusters (McDonald et al. 2013), finding them to be consistent with a comparable CC fraction (29 ± 7 per cent) in the common redshift range.

(vi) A possible origin of the discrepancy between the CC fraction in SZ-selected and X-ray-selected samples is the CC bias (Eckert et al. 2011). We tested this hypothesis with simulations of the CC bias: starting from a realistic population of clusters with the distribution of concentration parameters in the Planck sample, we simulate the ME-MACS selection and measure the CC fraction in the output sample (Section 5.2). Starting from a CC fraction of 29 per cent in the input population, we obtain a CC fraction of 48 per cent in the output sample, showing that CC bias plays a large role in the difference between the two samples. Nonetheless, according to our simulation, the probability of obtaining simultaneously two CC fractions of 29 per cent in Planck and 59 per cent in ME-MACS is only 0.2 per cent.

(vii) We considered several mechanisms that could also possibly affect SZ surveys to be biased against CC, namely the presence of radio galaxies in CCs, the role of shocks in increasing the SZ signal, the large Planck beam favouring the detection of multiple disturbed objects and a difference in the pressure profile at large radii. However, none of them seem sufficient to explain the difference between the observed CC fraction in ME-MACS and the one in Planck.

(viii) We noticed that the Planck sample hosts a population of objects, which, according to their expected luminosity (from L–Y scaling relation), should be present also in ME-MACS, but are not, since their observed luminosity is below the luminosity cut in that sample. Most of these X-ray underluminous objects are classified as NCC. The presence of this population of clusters, whose origin and properties are still unclear, in the Planck sample could possibly contribute to the difference.

ACKNOWLEDGEMENTS

We dedicate this paper to our colleague Y.Y. Zhang: we are indebted to her work (Zhang et al. 2011) for the analysis discussed in Paper I, on which this paper is based. We thank H. Ebeling for useful information about the ME-MACS sample and T. Reiprich for providing the concentration parameters of HIFLUGCS clusters.

REFERENCES

Arnaud M., Pointecouteau E., Pratt G. W., 2005, A&A, 441, 893
Battaglia N., Bond J. R., Pfrommer C., Sievers J. L., 2012, ApJ, 758, 74
Bleem L. E. et al., 2015, ApJS, 216, 27
Böhringer H. et al., 2000, ApJS, 129, 435
Böhringer H. et al., 2004, A&A, 425, 367
Böhringer H. et al., 2007, A&A, 469, 363
Burenin R. A., Vikhlinin A., Hornstrup A., Ebeling H., Quintana H., Mescheryakov A., 2007, ApJS, 172, 561
Cavagnolo K. W., Donahue M., Voit G. M., Sun M., 2009, ApJS, 182, 12
Chen Y., Reiprich T. H., Böhringer H., Ikebe Y., Zhang Y.-Y., 2007, A&A, 466, 805
David L. P., Kempner J., 2004, ApJ, 613, 831
Ebeling H., Edge A. C., Henry J. P., 2001, ApJ, 553, 668
Eckert D., Molendi S., Paltani S., 2011, A&A, 526, A79
Eckert D. et al., 2012, A&A, 541, A57
Fakhouri O., Ma C.-P., Boylan-Kolchin M., 2010, MNRAS, 406, 2267
Finoguenov A., Henriksen M. J., Miniati F., Briel U. G., Jones C., 2006, ApJ, 643, 790
Fraley C., Raftery A. E., 2002, J. Am. Stat. Assoc., 97, 611
Fraley C., Raftery A. E., Murphy T. B., Scrucca L., 2012, mclust Version 4 for R: Normal Mixture Modeling for Model-Based Clustering, Classification, and Density Estimation. Technical Report No. 597, Univ. Washington, WA
Girardi M., Boschin W., Barrena R., 2006, A&A, 455, 45
Hasselfield M. et al., 2013, J. Cosmol. Astropart. Phys., 7, 8
Horner D. J., Perlman E. S., Ebeling H., Jones L. R., Scharf C. A., Wegner G., Malkan M., Maughan B., 2008, ApJS, 176, 374
Hudson D. S., Mittal R., Reiprich T. H., Nulsen P. E. J., Andernach H., Sarazin C. L., 2010, A&A, 513, A37
Kass R. E., Raftery A. E., 1995, Journal of the American Statistical Association, 90, 773
Krause E., Pierpaoli E., Dolag K., Borgani S., 2012, MNRAS, 419, 1766
Lin H. W., McDonald M., Benson B., Miller E., 2015, ApJ, 802, 34
McDonald M., Benson B. A., Vikhlinin A., Stalder B., Bleem L. E., de Haan T., Lin H. W., Aird K. A., 2013, ApJ, 774, 23
Mann A. W., Ebeling H., 2012, MNRAS, 420, 2120 (ME-MACS)
Mantz A., Allen S. W., Ebeling H., Rapetti D., Drlica-Wagner A., 2010, MNRAS, 406, 1773
Mantz A. B., Allen S. W., Morris R. G., Schmidt R. W., von der Linden A., Urban O., 2015, MNRAS, 449, 199
Menanteau F. et al., 2012, ApJ, 748, 7
Motl P. M., Hallman E. J., Burns J. O., Norman M. L., 2005, ApJ, 623, L63
Nurgaliev D. et al., 2016, ApJ, preprint (arXiv:1609.00375)
Pascut A., Ponman T. J., 2015, MNRAS, 447, 3723
Perlman E. S., Horner D. J., Jones L. R., Scharf C. A., Ebeling H., Wegner G., Malkan M., 2002, ApJS, 140, 265

Pesce J. E., Fabian A. C., Edge A. C., Johnstone R. M., 1990, MNRAS, 244, 58
Pierre M. et al., 2016, A&A, 592, A1
Piffaretti R., Arnaud M., Pratt G. W., Pointecouteau E., Melin J.-B., 2011, A&A, 534, A109
Pipino A., Pierpaoli E., 2010, MNRAS, 404, 1603
Planck Collaboration VIII, 2011, A&A, 536, A8
Planck Collaboration IX, 2011, A&A, 536, A9
Planck Collaboration V, 2013, A&A, 550, A131
Planck Collaboration VI, 2013, A&A, 550, A132
Planck Collaboration XX, 2014, A&A, 571, A20
Planck Collaboration XXVIII, 2014, A&A, 571, A28
Planck Collaboration XXIX, 2014, A&A, 571, A29
Planck Collaboration XXVII, 2016, A&A, 594, A27
Pratt G. W., Croston J. H., Arnaud M., Böhringer H., 2009, A&A, 498, 361
Pratt G. W. et al., 2010, A&A, 511, A85
R Core Team 2015, R: A Language and Environment for Statistical Computing. R Foundation for Statistical Computing, Vienna, Austria. (Available at: https://www.R-project.org).
Raftery A. E., 1995, Bayesian Model Selection in Social Research: Sociological Methodology, Vol. 25. American Sociological Association, Washington, D. C., p. 111
Reiprich T. H., Böhringer H., 2002, ApJ, 567, 716
Rosati P., Della Ceca R., Norman C., Giacconi R., 1998, ApJ, 492, L21
Rosati P., Borgani S., Norman C., 2002, ARA&A, 40, 539
Rossetti M., Molendi S., 2010, A&A, 510, A83
Rossetti M. et al., 2016, MNRAS, 457, 4515 (Paper I)
Sanderson A. J. R., Edge A. C., Smith G. P., 2009, MNRAS, 398, 1698
Santos J. S., Rosati P., Tozzi P., Böhringer H., Ettori S., Bignamini A., 2008, A&A, 483, 35
Santos J. S., Tozzi P., Rosati P., Böhringer H., 2010, A&A, 521, A64
Sayers J. et al., 2013a, ApJ, 764, 152
Sayers J. et al., 2013b, ApJ, 768, 177
Schwarz G., 1978, Ann. Stat., 6, 461
Semler D. R. et al., 2012, ApJ, 761, 183
Sereno M., 2015, MNRAS, 450, 3665
Snowden S. L., Mushotzky R. F., Kuntz K. D., Davis D. S., 2008, A&A, 478, 615
Sommer M. W., Basu K., 2014, MNRAS, 437, 2163
Sunyaev R. A., Zeldovich Y. B., 1970, Comments Astrophys. Space Phys., 2, 66
Sunyaev R. A., Zeldovich Y. B., 1972, Comments Astrophys. Space Phys., 4, 173
Tinker J., Kravtsov A. V., Klypin A., Abazajian K., Warren M., Yepes G., Gottlöber S., Holz D. E., 2008, ApJ, 688, 709
Venables W. N., Ripley B. D., 2002, Modern Applied Statistics with S, 4th edn. Springer-Verlag, New York
Vikhlinin A. et al., 2009, ApJ, 692, 1060
Voges W. et al., 1999, A&A, 349, 389
Zhang Y.-Y., Andernach H., Caretta C. A., Reiprich T. H., Böhringer H., Puchwein E., Sijacki D., Girardi M., 2011, A&A, 526, A105

SUPPORTING INFORMATION

Supplementary data are available at *MNRAS* online.

Table 1. Properties of the clusters in our Planck sample. Column (1) is the INDEX in the PSZ1 catalogue, column (2) the Planck name, column (3) provides an alternative name, columns (4) and (5) are the coordinates of the X-ray peak that we used to measure the concentration parameter, columns (6) and (7) are the redshift and mass as provided in the Planck catalogue, columns (8) and (9) are the concentration parameter and its error, while in column (10) we list the ID of the observations used in our analysis (those starting with ‘0’ are *XMM–Newton* data).

Table 2. Properties of the clusters in the ME-MACS sample. Column (1) is the cluster name, columns (2) and (3) are the coordinates of the X-ray peak that we used to measure the concentration parameter, column (4) is the redshift of the clusters, column (5) is its mass calculated from the X-ray luminosity in Mann & Ebeling (2012), columns (6) and (7) are the concentration parameter and its error, while in column (8) we list the ID of the observations used in our analysis (those starting with ‘0’ are *XMM–Newton* data.

APPENDIX A: CORRELATION WITH $D_{\text{X-BCG}}$

As discussed in Section 1, the concentration parameter is an indicator of the presence of a CC, while the indicator used in Paper I, that is, $D_{\text{X-BCG}}$ the projected distance between the X-ray peak and the BCG, is an indicator of dynamical activity. CCs are usually found in dynamically relaxed systems and $D_{\text{X-BCG}}$ has been shown to correlate with thermodynamical indicators of the CC state (Sanderson et al. 2009). Here, we test the correlation between $D_{\text{X-BCG}}$ and c for the Planck and ME-MACS samples. For Planck, we used the values in Paper I for the 122 common clusters, while for ME-MACS we used the values provided for the full sample in Mann & Ebeling (2012). The correlation plot is shown in Fig. A1, where we also show the threshold values that we used to classify clusters in CC/NCC here and relaxed/disturbed in Paper I ($D_{\text{X-BCG}} = 0.02\,R_{500}$). We performed the Spearman and Kendall correlations test on both samples separately and on the joint sample. The results are shown in Table A1 . In both data sets, separately and in the joint one, we find a significant anticorrelation between the two indicators, with most relaxed clusters being also CC and disturbed ones being NCC. The correlation is stronger for ME-MACS than for Planck, which hosts

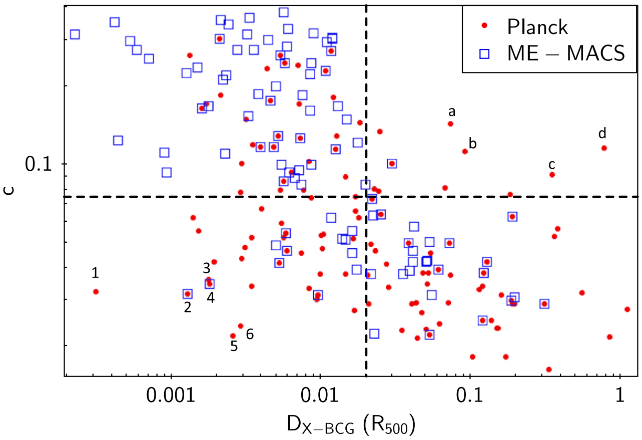

Figure A1. Distribution in the $D_{\text{X-BCG}}$–c plane of Planck (red circles) and ME-MACS (blue open squares) clusters. Dashed lines mark the separation between CC/NCC and relaxed/disturbed clusters. Objects in the upper-left quadrant are relaxed CC, while in the lower quadrant lie disturbed NCC systems.

Table A1. Output of correlation tests.

Sample	Spearman ρ	p_0	Kendall τ	p_0
Planck	−0.43	6×10^{-7}	−0.30	8×10^{-7}
ME-MACS	−0.74	2×10^{-19}	−0.54	4×10^{-16}
Joint	−0.60	2×10^{-23}	−0.43	–

a larger number of outliers, that is, clusters classified as relaxed but without a CC (possibly for projection effects) and disturbed objects with a CC. We investigated one by one the most outstanding outliers in the plot, which we label with numbers and letters in Fig. A1, with the aim of trying to understand if their presence in Planck but not in ME-MACS may be related to selection effects. The lower-left quadrant of the plot contains clusters classified as 'relaxed NCC': as discussed in Paper I, we expect that 7.5 per cent of the clusters classified as relaxed by $D_{\rm X,\,BCG}$ are in fact disturbed object where the separation between the X-ray peak and the BCG occurs mainly along the line of sight. Moreover, an intrinsic limitation of the dynamical indicator $D_{\rm X\text{-}BCG}$ is that not all mergers, and not all phases of the mergers, cause an offset between the BCG and the X-ray peak. The most deviating outliers in this panel are: (1) A2147 (Hudson et al. 2010, $z = 0.03$), (2) A1758N (David & Kempner 2004, $z = 0.27$, also in ME-MACS), (3) A3266 (Finoguenov et al. 2006, $z = 0.05$), (4) A697 (Girardi, Boschin & Barrena 2006, $z = 0.28$, also in ME-MACS), (5) A119 (Hudson et al. 2010, $z = 0.05$) and (6) A1437 ($z = 0.13$, little X-ray information is available in the literature, our own analysis shows a disturbed and elongated morphology). Visual inspection of their X-ray images shows that they are all clearly disturbed objects undergoing mergers, as also supported by the literature. Most of them are simply not in ME-MACS because they are local systems ($z < 0.15$), while the only two objects at $z > 0.15$ are also found in ME-MACS.

The upper-right panel contains object classified as 'disturbed CC' and is populated mainly by Planck objects. The most deviating objects are: (a) RXC J0232.2−4420 (see the image in the ACCEPT archive Cavagnolo et al. 2009, $z = 0.28$), (b) RXC J0638.7−5358 (see the image in the ACCEPT archive Cavagnolo et al. 2009, $z = 0.22$), (c) SPT-CL J0411−4819 (McDonald et al. 2013, $z = 0.43$) and (d) ACT-CL J0102−4915 a.k.a. El Gordo (Menanteau et al. 2012, $z = 0.89$). It is interesting to note that all these clusters feature a significant surface brightness peak in an overall disturbed X-ray morphology. El Gordo is probably the most striking example: Menanteau et al. (2012) show that it is undergoing a major merger but it preserves a bright region with cool, low entropy and high metal abundance gas, likely the 'CC remnant' (Rossetti & Molendi 2010) of one of the merging substructures. Similar systems should be in principle easily detected also in X-ray surveys; however, they are not in ME-MACS simply because they do not fall in the sky area surveyed by MACS ($\delta > -40$; Mann & Ebeling 2012).

Analysis of the outliers in this relation could have been in principle very useful to suggest possible selection effects but we are unfortunately limited by the incomplete spatial and redshift overlap of the two surveys, as discussed also in Section 5.1.

This paper has been typeset from a TEX/LATEX file prepared by the author.